

# Numerical method study of how buildings affect the flow characteristics of an urban canopy

Ning Zhang<sup>†</sup> and Weimei Jiang<sup>‡</sup>

*Department of Atmospheric Science, Nanjing University, Nanjing, 210093 China*

Fei Hu<sup>‡</sup>

*Key Laboratory of Atmospheric Physics and Chemistry, Institute of Atmospheric Physics,  
Chinese Academy of Sciences, Beijing, 100029 China*

*(Received June 25, 2003, Revised September 18, 2003, Accepted March 29, 2004)*

**Abstract.** The study of how buildings affect wind flow is an important part of the research being conducted on urban climate and urban air quality. NJU-UCFM, a standard  $k$ - $\epsilon$  turbulence closure model, is presented and is used to simulate how the following affect wind flow characteristics: (1) an isolated building, (2) urban canyons, (3) an irregular shaped building cluster, and (4) a real urban neighborhood. The numerical results are compared with previous researchers' results and with wind tunnel experiment results. It is demonstrated that the geometries and the distribution of urban buildings affect airflow greatly, and some examples of this include a changing of the vortices behind buildings and a "channeling effect". Although the mean air flows are well simulated by the standard  $k$ - $\epsilon$  models, it is important to pay attention to certain discrepancies when results from the standard  $k$ - $\epsilon$  models are used in design or policy decisions: The standard  $k$ - $\epsilon$  model may overestimate the turbulence energy near the frontal side of buildings, may underestimate the range of high turbulence energy in urban areas, and may omit some important information (such as the reverse air flows above the building roofs). In ideal inflow conditions, the effects of the heights of buildings may be underestimated, when compared with field observations.

**Keywords:** urban micro-climate; building; numerical simulation; urban canopy.

---

## 1. Introduction

Increasing populations and industrial activities have resulted in serious pollution problems in urban areas. The toxic materials generated from vehicles, heating and cooling systems of buildings, sudden fires, and other urban activities can sicken or cause fatal harm to humans living within a polluted area. Even worse, acts of terrorism can result in terrible consequences for people in populated areas. In order to minimize the effects of these dangers, it is necessary to understand the characteristics of urban airflow, to be able to predict the pollutant dispersion in a given urban area.

The climate of urban canopies is controlled mainly by a micro-meteorological urban canopy system, rather than the meso-scale forces controlling boundary layer climates. The urban canopy is

---

<sup>†</sup> Ph. D. Student

<sup>‡</sup> Professorr

composed of basic elements, such as isolated buildings, building clusters, and street canyons. The study of the shape, orientation, and distribution of buildings and their effects on airflows around them can improve our understanding of urban flow characteristics and pollutant distributions in urban areas.

Many investigations have been carried out using wind tunnels or numerical models to study the airflow around isolated buildings and in urban canyons (Hosker 1985, Baik and Kim 1999, Kim and Baik 1999, Ashie 1999). A great amount of information on such flow structures has been gathered. For instance we now understand that because of a building's effect on airflow, there will be separation and reattachment of airflows at the top of the building and re-circulations at the upwind and downwind sides of the building.

The flow regimes in urban street canyons can be categorized into the following: the isolated roughness flow, the wake interference flow, and the skimming flow. These flow regimes are determined by the degree of interaction between the vortex generated behind a given upwind building and a given downwind building (Hussain and Lee 1980, Oke 1988, Hunter 1992, Sini 1996). In three-dimensional terms, the height-to-length ratio and the height-to-width ratio in an urban canyon are crucial factors for determining flow regime. In two-dimensional terms, the height-to-width ratio is a crucial factor determining flow regime. If the buildings are well apart, a low-pressure recirculation vortex is formed behind the upwind building due to the flow separation at the building top edge, and a bolster eddy vortex is formed because of the flow separation on the downwind wall (Sini 1996). With an isolated roughness flow, the flow recovers its upwind profile before it meets a downwind building, and the interaction between the two vortices (two co-rotating vortices) is negligible. If the buildings are closer, however, the downwind building disturbs the recirculation vortex before readjustment can take place, making interaction between the two vortices possible, which will produce a wake interference flow. If the street canyon becomes narrow, the bulk of the above-roof flow does not enter the canyon, and a stable vortex is established in the canyon, producing a skimming flow.

New investigations into irregular shaped buildings and the effects of building clusters on airflow are currently underway, and a numerical simulation is a cost-effective method for carrying out such investigations. Currently, most of these studies are carried out with numerical methods or in wind tunnels. In most numerical models, the effect of buildings is parameterized, rather than explicitly solved.

In our study, a series of numerical simulations on how buildings affect airflows are introduced. A standard  $k-\varepsilon$  turbulence closure model, NJU-UCFM (Nanjing University Urban Canopy Flows Model) is presented and it used to simulate in detail the effects on flows characteristics of the following: (1) an isolated building, (2) urban canyons, (3) an irregular shaped building cluster; and (4) a real neighborhood. The results are compared with the results of previous numerical studies and with the results of wind tunnel experiments.

## 2. Description of the numerical model

NJU-UCFM is a  $k-\varepsilon$  turbulence closure model, which solves the Navier-Stokes equations by using two further differential equations to effect closure.

The equations used are as follows:  
three momentum equations:

$$\frac{\partial U_i}{\partial t} + U_j \frac{\partial U_i}{\partial x_j} = \frac{\partial}{\partial x_j} \left[ v_t \frac{\partial U_i}{\partial x_j} \right] - \frac{\partial P}{\partial x_i}; i = 1, 2, 3 \quad (1)$$

a continuity equation:

$$\frac{\partial U_j}{\partial x_j} = 0 \quad (2)$$

an equation of the transportation of turbulence kinetic energy:

$$\frac{\partial k}{\partial t} + U_j \frac{\partial k}{\partial x_j} = \frac{\partial}{\partial x_j} \left[ \frac{v_t}{\sigma_k} \frac{\partial k}{\partial x_j} \right] + v_t \frac{1}{2} \left[ \frac{\partial U_i}{\partial x_j} + \frac{\partial U_j}{\partial x_i} \right]^2 - \varepsilon \quad (3)$$

an equation for the dissipation of turbulence kinetic energy:

$$\frac{\partial \varepsilon}{\partial t} + U_j \frac{\partial \varepsilon}{\partial x_j} = \frac{\partial}{\partial x_j} \left[ \frac{v_t}{\sigma_\varepsilon} \frac{\partial \varepsilon}{\partial x_j} \right] + c_1 c_\mu k \frac{1}{2} \left[ \frac{\partial U_i}{\partial x_j} + \frac{\partial U_j}{\partial x_i} \right]^2 - c_2 \frac{\varepsilon^2}{k} \quad (4)$$

where:

$U_i, i=1, 2, 3$  is wind velocity;

$P \left( = \frac{\bar{P}}{\rho} + \frac{2}{3} k \right)$  is augmented pressure;

$k = \frac{1}{2} \overline{u_j u_j}$  is turbulent kinetic energy;

$\varepsilon \left( = v \frac{\partial u_i}{\partial x_j} \frac{\partial u_i}{\partial x_j} \right)$  is the dissipation of turbulent kinetic energy;

$v_t \left( = c_\mu \frac{k^2}{\varepsilon} \right)$  is turbulent viscosity, and

$c_\mu, c_1, c_2, \sigma_k, \sigma_\varepsilon$  are constants (Paterson and Apelt 1986, 1989). The constants are specified as (0.09, 1.44, 1.92, 1.0, 1.3) (Sini 1996).

The equations are solved in a Cartesian coordination and the computational domain is constructed of a non-uniformly spaced staggered mesh system. Fine mesh resolution is used to surround the building vicinity, and the mesh size is increased relative to the distance to the building. The total grid points are adjusted for different simulated objects. The above equations set is solved with the SIMPLE (Semi-Implicit Method for Press-Linked Equation) algorithm, described by Patankar (1980). Using this algorithm, at each time step the tentative horizontal and vertical velocities are first obtained under an assumed pressure field. Then, the pressure change needed to adjust the velocity field to satisfy the mass continuity is calculated by solving a pressure-Poisson equation. The final velocity and pressure fields are computed by using the velocity and pressure correction equations, respectively.

The initial condition and inflow boundary condition for the wind velocities, the turbulent kinetic energy and the its dissipation are specified as follows:

$$U_0 = U_{ref} \left( \frac{z}{z_{ref}} \right)^\alpha \quad (5)$$

$$k_0 = 0.0003u_0^2 \quad (6)$$

$$\varepsilon_0 = \frac{C_\mu^{3/4}k_0^{3/2}}{\kappa z} \quad (7)$$

In Eq. (5),  $U_{ref}$  is the reference wind speed at the reference height  $z_{ref}$ , and  $\alpha$  is the power exponent for the wind profile. A free outlet boundary condition is used at the side, the top, and the outflow conditions. The wall function approach of Launder and Spalding (1974) is used to bridge the viscosity-affected region between the wall and the fully turbulent region. In accordance with the Launder and Spalding method, a linearized source term is modified, based on wall shear stress, which can be calculated by the following:

$$U^* = \frac{1}{\kappa} \ln(Ey^*) \quad (8)$$

where

$$U^* \equiv \frac{U_N C_\mu^{1/4} k_N^{1/2}}{\tau_w / \rho} \quad (9)$$

$$y^* \equiv \frac{\rho C_\mu^{1/4} k_N^{1/2} y_N}{\mu} \quad (10).$$

$U_N$  is the time averaged velocity at node  $N$  in the viscosity-affected near wall region,  $E$  is the boundary layer constant, approximately equal to 9.0,  $k_N$  is the turbulence energy at node  $N$ ,  $y_N$  is the distance between the node  $N$  and the solid boundary, and  $\mu$  is the dynamic viscosity of the fluid. The boundary condition of  $k$  at the wall is imposed as:

$$\frac{\partial k}{\partial n} = 0 \quad (11)$$

where  $n$  is the local coordinate normal to the wall. The  $\varepsilon$  at the wall adjacent cells is computed by using Eq. (7) and  $z$  in Eq. (7) is replaced by  $y_N$ .

### 3. Analysis of simulated results

#### 3.1. Simulation of isolated building and urban canyons

Flow structures around an isolated building is simulated,  $U_{ref}=6.0$  m/s,  $z_{ref}=100$  m,  $\alpha=0.21$  in Eq. (5), inlet direction is along  $x$  direction. The finest grid is 1 m.

The vectors of the horizontal plane at 0.28 H (where H is the building height) and the vertical plane are shown in Fig. 1 and Fig. 2. Upwind of the building is a “displacement zone”, where the fluid particles are first influenced by the presence of the building. A small vortex appears near the upwind wall. In this zone, both the speed and the direction of the wind will be affected, as the flow attempts to travel around and over the building. A turbulence recirculation zone (cavity zone) appears beyond the building, where a double vortex circulation is shown. The width of the cavity is similar to the width of the building, and the cavity closure point is 2 H from the downwind wall of the building.

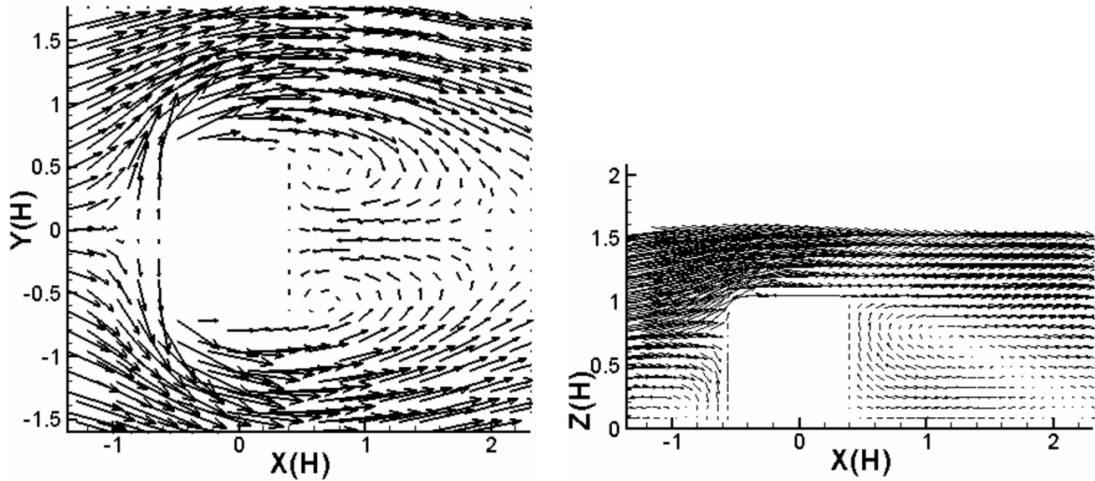


Fig. 1 Horizontal plane view of the wind vectors at 0.28H around an isolated building (numerical result) Fig. 2 Vertical vectors around an isolated building (section along the line  $y=0$ ) (numerical result)

The simulated mean airflow agrees well with the results of Hosker (1985). A comparison is made between the numerical result and the result of a CEDVAL wind tunnel experiment at Hamburg University<sup>[1]</sup>. The simulated reattachment point location and the cavity zone flow structure are the same as those in the CEDVAL experiment. In the simulated result, however, the reverse flow on the top of the building is very weak and it does not appear in Fig. 2. This is because the standard  $k-\epsilon$  model may overestimate the turbulence energy near the frontal side of the building. This will be made evident in Sec. 3.2, where the numerical simulated turbulence energy distribution will be compared with that of the wind tunnel experiment result. The overestimation of turbulence energy

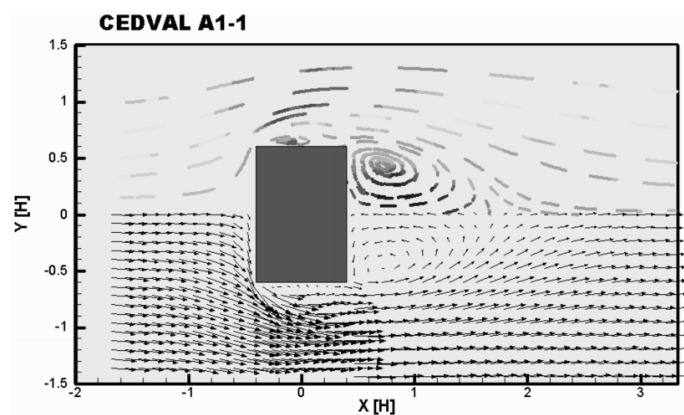


Fig. 3 Horizontal plane view of the wind vectors at 0.28H around an isolated building (wind tunnel experiment result, CEDVAL, Hamburg University)

<sup>[1]</sup>More information can be found at <http://www.mi.uni-hamburg.de>

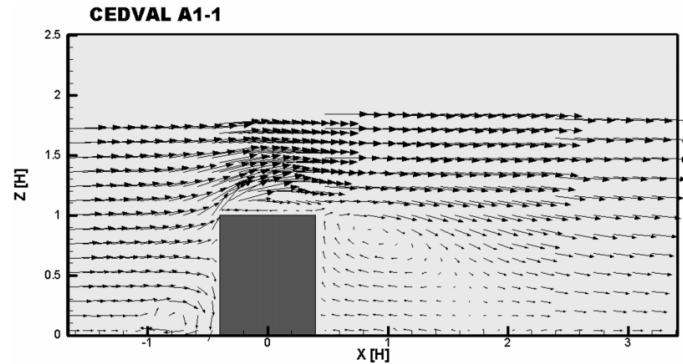


Fig. 4 Vertical vectors around an isolated building (section along the line  $y=0$ ) (wind tunnel experiment result, CEDVAL, Hamburg University)

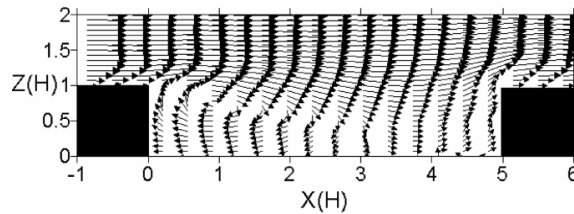


Fig. 5 Simulated "isolated roughness" flow

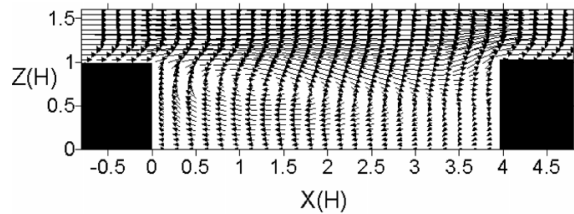


Fig. 6 Simulated "wake interference" flow

near the frontal side gives rise to the large eddy viscosity, and this viscosity will eliminate the reverse flow on the roof.

In three-dimension terms, it is generally accepted that the relative height ( $H$ ), width ( $W$ ), and length ( $L$ ) of a canyon are the important determining factors of flow regime. Figs. 5, 6, 7, and 8 are the flow regimes when  $L/H=7$  and  $H/W=0.25, 0.5, 1.0,$  and  $2.0$ , respectively. In Fig. 5, amid the widely spaced buildings, the flow returns to the upwind profile before the downwind building is encountered, and is described as an "isolated roughness" flow. Fig. 6 is a "wake interference" flow, where the downwind building disturbs the adjustment of the wind. Both Fig. 7 and Fig. 8 are "skimming" flows. In Fig. 8, the canyon is narrow enough that the vortex is broken into three parts.

If the problems associated with urban canyon climates, such as high pollution concentrations, are to be minimized, then knowledge of the threshold  $H/W$  ratios of different  $L/H$  for the transition flow regimes is important. The threshold ratios of  $H/W$  for different  $L/H$  are estimated with our model, using a 30-minute averaged result. Normally, the time scale of flows around buildings is

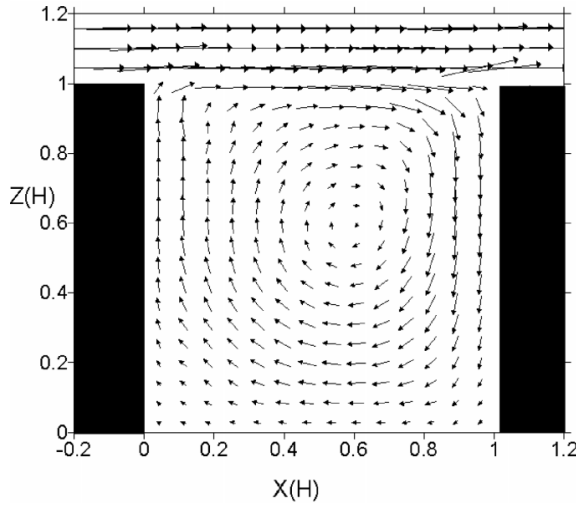


Fig. 7 Simulated “skimming” flow (a)

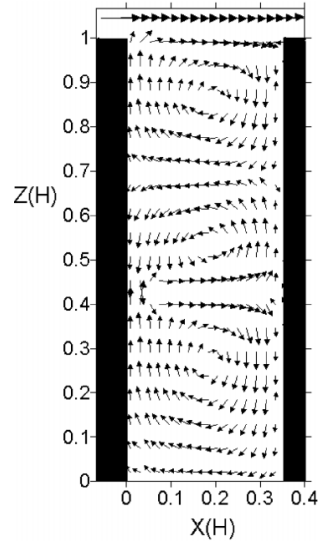


Fig. 8 Simulated “skimming” flow (b)

Table 1 Threshold  $H/W$  for different  $L/H$

$L/H$	“skimming” flow to “wake interference” flow			“wake interference” flow to “isolated roughness” flow		
	NJU-UCFM	Oke	Hunter	NJU-UCFM	Oke	Hunter
3	0.75	0.75	0.74	0.25	0.38	0.24
7	0.70	0.75	0.67	0.20	0.20	0.22
10	0.70			0.20		

several minutes. A 30-minute averaged result can be trusted to grasp the characteristics of the flow regimes. The results are compared in Table 1, along with the results from Oke (1988) (a wind tunnel experiment result) and Hunter (1992) (a numerical result from a steady-state  $k-\epsilon$  closure model). Our model can simulate the flow structures well for different flow regimes.

### 3.2. Simulation of a complex buildings cluster

In this section, we discuss the simulation of a complex buildings cluster, which includes three complex buildings. The geometries of the buildings are similar to a “V” shape, as shown in Fig. 9. The axis of  $x$  is from west to east, and the axis of  $y$  is from south to north. The heights of the buildings are 40 m each. The domain size is 200 m  $\times$  200 m. The inlet flow is north, and the parameters in Eq. (5) are as follows:  $U_{ref}=2.0$  m/s,  $z_{ref}=10$  m,  $\alpha=0.2$ . The finest grid is 3 m.

The physical simulation of the same inlet flow condition is carried out in an NJU environment wind tunnel. An introduction to this wind tunnel experiment can be found in Appendix A.

Fig. 10 and Fig. 11 show the horizontal wind vectors and the horizontal contour lines of the scale wind speed. A high wind speed area appears between the buildings in both the numerical simulation result and the physical simulation result. The maximum speed in this area is 2.86 m/s in the wind

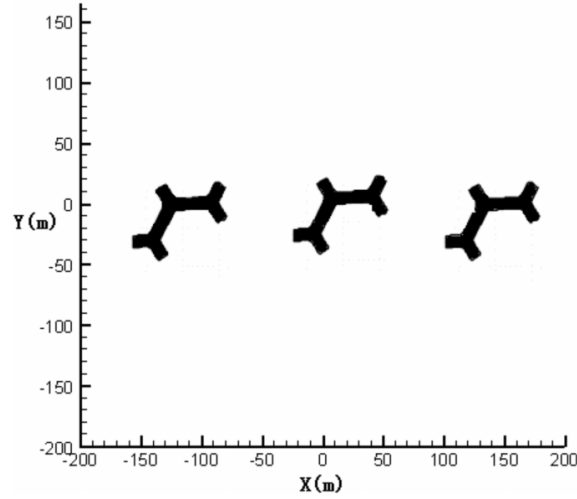


Fig. 9 The simulation domain of a three irregular building cluster

tunnel result and 2.5 m/s in the numerical simulation. This condition can be described as a “channeling effect”. In other areas around the buildings the wind speed decreases. In the direction of  $x$  the width of low wind speed zone is equal to the total cross wind width of the buildings. In the upwind direction, the effect of the buildings can be  $2H$  in the direction of  $x$ . If the buildings were regular (such as a buff body or a cylinder), a double vortex circulation would be found on the downwind side of the buildings. Because of the irregular geometry of the buildings, only one vortex appears behind the building.

Fig. 12 and Fig. 13 illustrate the horizontal distribution of turbulence energy at 8 m from both the numerical result and the wind tunnel experiment result. In the case of the numerical result, the value of  $k$  is overestimated on the frontal side of the buildings and it is underestimated, both in intensity and in range, in the recirculation area behind the buildings, in comparison with the physical simulation

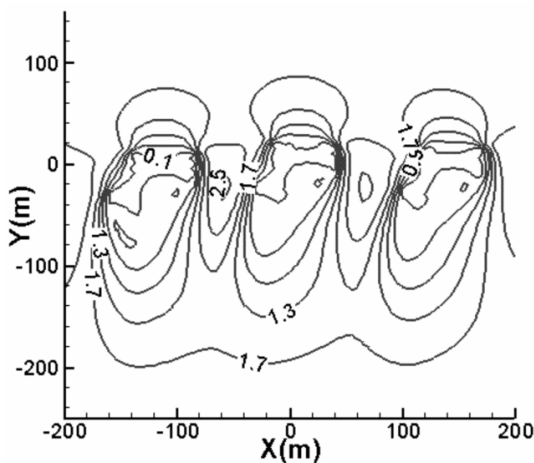


Fig. 10 Horizontal wind speed around the buildings at 8 m (Unit: m/s)

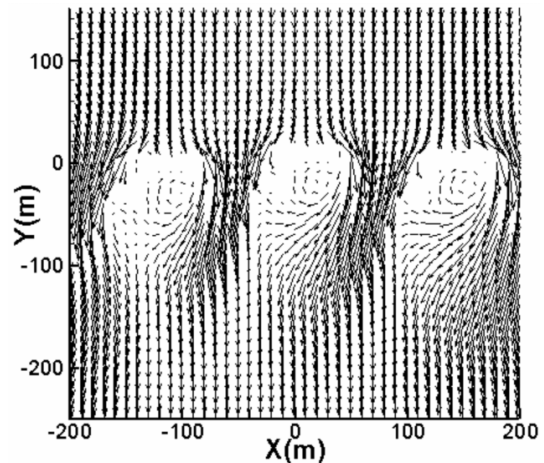


Fig. 11 Horizontal wind vectors around the buildings at 8 m

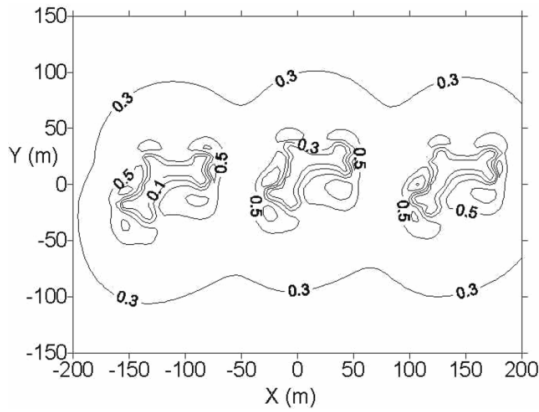


Fig. 12 Horizontal distribution of turbulence energy at 8 m (numerical result)

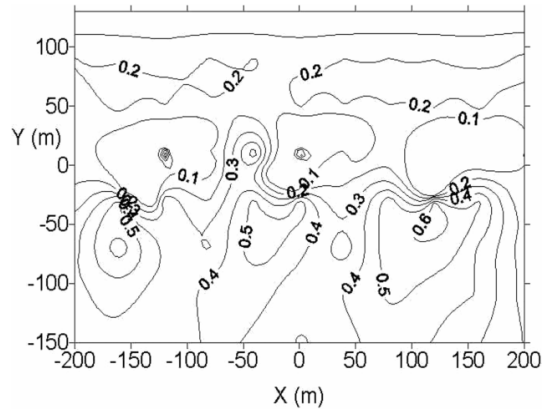


Fig. 13 Horizontal distribution of turbulence energy at 8 m (wind tunnel experiment result in NJU)

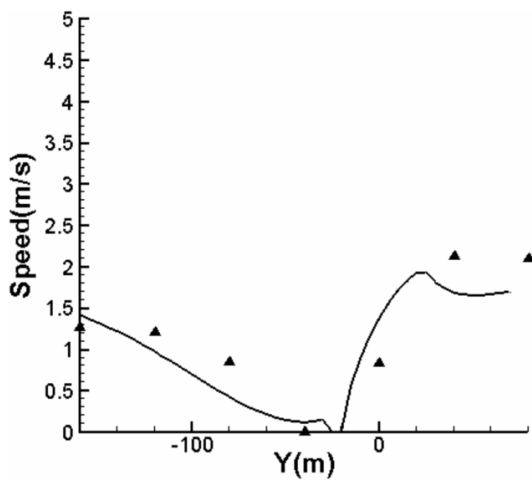


Fig. 14 Horizontal scale wind speed along y direction through a point (x: 0 m; z: 20 m) (solid line for numerical simulation result and triangles for wind tunnel experiment result in NJU)

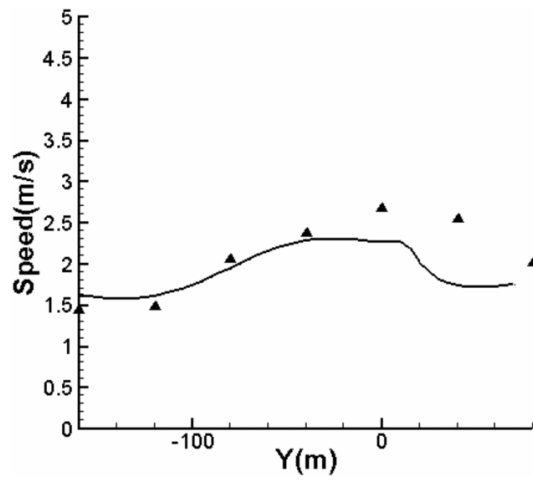


Fig. 15 Horizontal scale wind speed along y direction through a point (x: 80 m; z: 20 m) (solid line for numerical simulation result and triangles for wind tunnel experiment result in NJU)

result. The reasons for these discrepancies, which are explained successfully by Murakami (1990), are related to the poor ability of the standard  $k-\epsilon$  models in calculating the structure of turbulence production and in reproducing of Karman's vortex. These inaccuracies are larger when the simulated objects are complex geometry buildings than when the simulated objects are regular bodies.

Fig. 14 is the scale wind speed distribution along the y axis through a point (x: 0 m, z: 20 m). The wind speed peaks on the windward side of the building, and behind the building the speed decreases dramatically for the block of buildings. At y=0 m the speed is zero, since this point is in the building. The physical simulation result agrees well with the numerical result. Fig. 15 is the wind speed distribution along the y axis through a point (x: 80 m, z: 20 m). The line crosses the space between the middle building and the east building. Because of the channeling effect, a speed

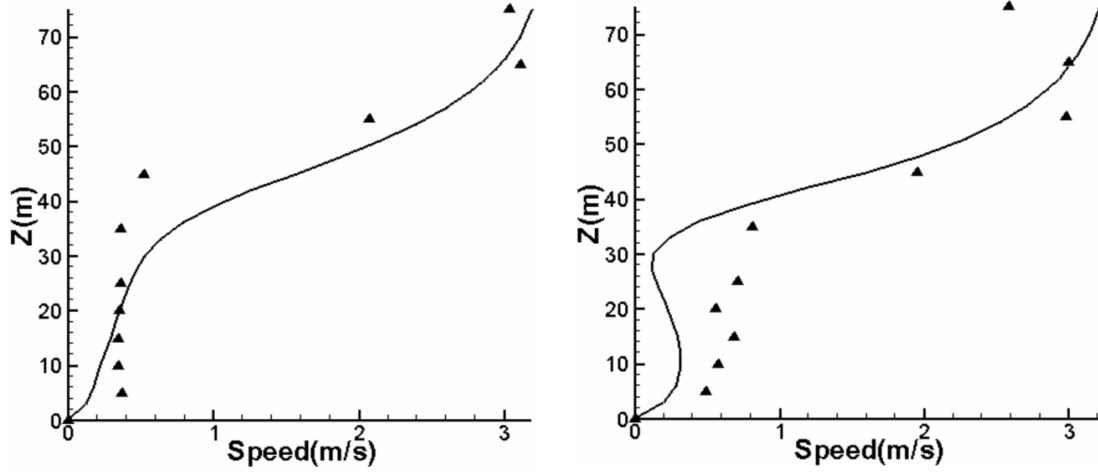


Fig. 16 Vertical scale wind speed profile at (x: -110 m; y: -40 m) (solid line for numerical simulation result and triangles for wind tunnel experiment result in NJU)

Fig. 17 Vertical scale wind speed profile at (x: -60 m; y: -20 m) (solid line for numerical simulation result and triangles for wind tunnel experiment result in NJU)

peak occurs in the space between the buildings, and this effect spreads to  $1.2 H$  in the vertical direction.

Fig. 16 and Fig. 17 are the vertical profiles at point (-110, -40) and point (-60, -20). Point (-110, -40) is in the cavity behind the west building. In the area under the height of building, the wind speed is low and the vertical change is small. Above the building, the wind speed increases greatly with height. Point (-60, -20) is between the buildings, and the “channeling effect” is evident, especially at the height of  $0.5H$ .

### 3.3. Simulation on a real neighborhood

In this section of the paper, we discuss the airflow structures of a real neighborhood when different inflow directions are simulated. The distribution of buildings in the neighborhood is shown in Fig. 18. The domain is 1250 m from west to east and 1200 m from south to north.  $U_{ref}=2.2$  m/s,  $z_{ref}=10$  m,  $\alpha=0.25$  in Eq. (5). The finest grid is 3 m. The inflow directions are west, north-west, and south-west.

Fig. 19, Fig. 20, and Fig. 21 illustrate the wind vectors at the height of 9 m, when the inflow directions are from the west, from the northwest, and from southwest. In the middle and in the southwest part of the neighborhood, the vectors are in disarray where the buildings are dense. In the north and southeast part of the area, the flows are regular, and the wind direction is same as the inflow direction. At the edge of the dense building cluster, the flow will travel around the buildings, and in the middle of this area, there are reverse vectors. Between the buildings, or building clusters, there are wind speed peak areas, which occur due to the “channeling effect”. Because of the friction and drag of the buildings in the dense building cluster, the wind speed loss is great, while the wind speed loss is less in the other areas. The airflows climb the windward walls of the buildings and descend behind them due to the blocking of the buildings.

The averaged vertical wind profiles of different inflow directions are shown in Fig. 20. The wind

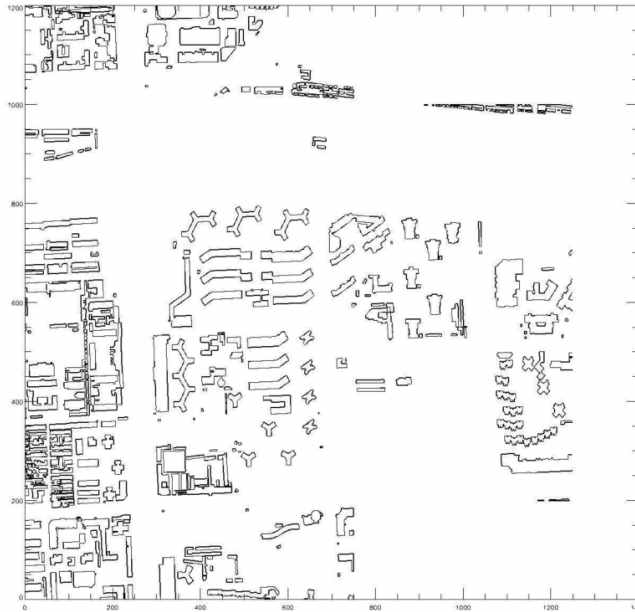


Fig. 18 Buildings distribution of the real neighborhood

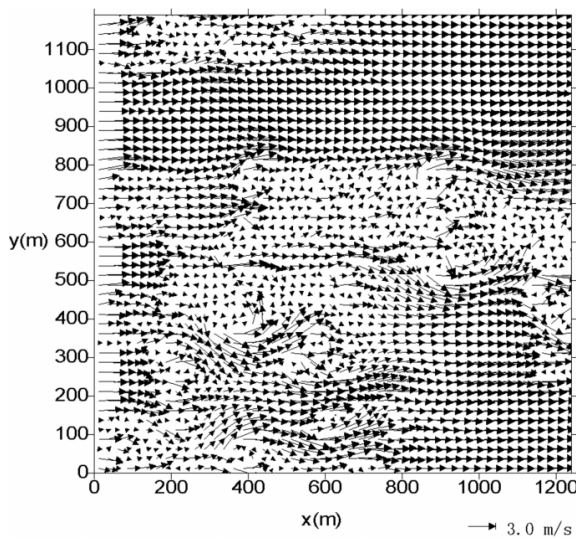


Fig. 19 Wind vectors at 9 m, west wind inflow

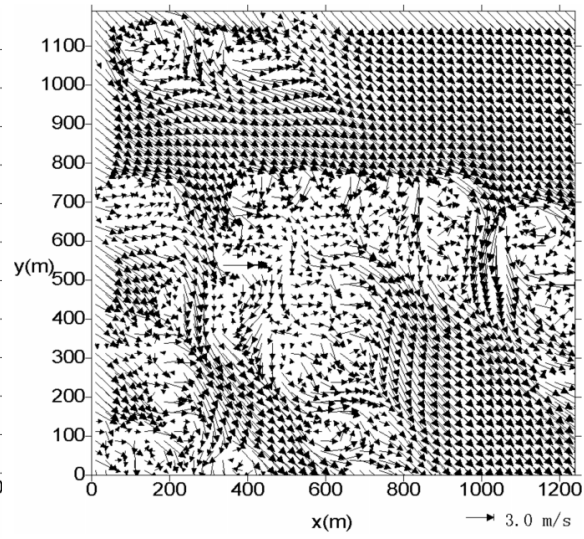


Fig. 20 Wind vectors at 9 m, northwest inflow

speed is of loss under 80 m (about 2 H, where H is the average building height) for each inflow direction. The wind speed loss is greatest at the height of 20 m (about 0.5 H). Below 20 m, the speed losses of the northwest and the west winds are greater than that of the southwest wind, while the speed loss of the southwest wind is greater above 20 m. This result shows that wind speed loss is related to the distribution of buildings and the wind direction. An advanced investigation should be conducted to study the relation in detail. Normally, the extension of a roughness sub-layer (RS)

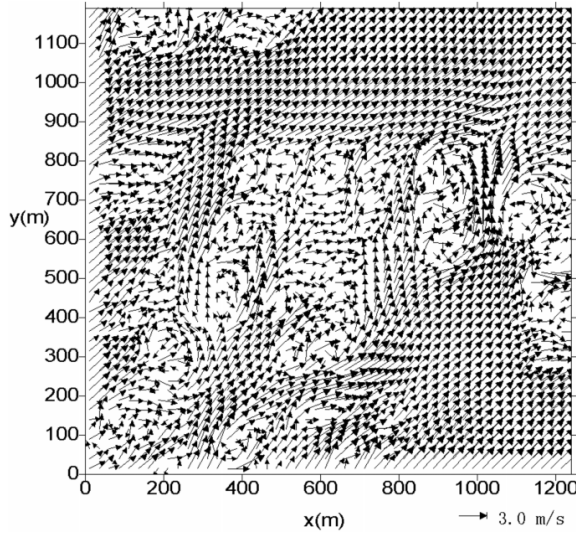


Fig. 21 Wind vectors at 9 m, south-west inflow

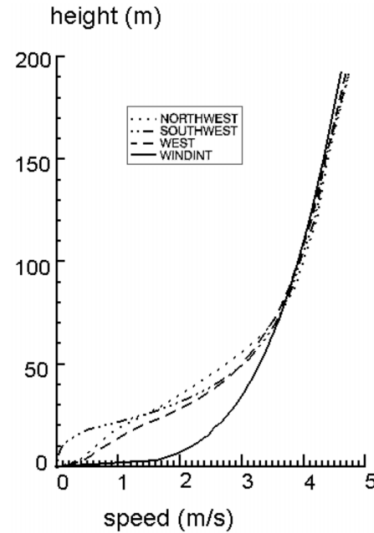


Fig. 22 The average wind profiles under different inflow conditions (the solid line represents the initial vertical wind speed profile; the dashed line represents the simulated averaged speed profile when the inflow is west; the dotted line represents the northwest inflow and dot-dot-dash line represents the southwest inflow)

will be a height of  $z=2-5h$  of field observations ( $h$  being the height of the roughness elements)(Rotach 1995), the simulated RS height is smaller than the result from Rotach as illustrated in Fig. 22. This result is mainly caused by the inflow conditions. In a field observation, the inflow is complex, fully turbulent, and affected by the buildings it is passing by, while in the numerical simulation an ideal and uniform flow is used. The inflow characteristics (including the mean flow profile and the turbulence characteristic) will play an important role in any further simulation of real conditions.

#### 4. Conclusions and discussion

A  $k-\varepsilon$  turbulence closure model was used to simulate the flow structures around urban buildings (including an isolated building, an urban canyon, a complex buildings cluster, and a real neighborhood). The presented model demonstrated the effect of buildings on fluid motion well. In the case of an isolated building, the displacement, cavity, and reattachment can be well simulated; but the location of the cavity and the reverse flow on the top of the building cannot be described well. For urban canyons, the model can describe the main type of the flow regimes: an “isolated roughness” flow, a “wake interference” flow, and a “skimming” flow. The threshold ratios of  $H/W$  are estimated and these estimates agree well with the results of previous studies. In the case of a complex buildings cluster, the channeling effect caused by the location and the geometries of the buildings greatly affect the airflow. According to our numerical results, the effects of building clusters on airflows reach a height of  $2H$  (where  $H$  is the average height of the buildings), which is

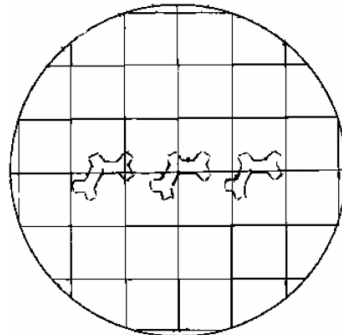


Fig. 23 Building models location in wind tunnel experiment

much lower than the field observation results. A reason for this might be the inability to simulate real inflow conditions.

The results from NJU-UCFM on mean airflows agree well with wind tunnel studies and other previous research, although some important information may be lost when using this method. The most important inaccuracies of this method are the overestimation of the turbulence energy near the frontal sides of buildings and the underestimation of the turbulence energy behind the buildings, when compared with physical simulations. Some new  $k-\varepsilon$  models, such as the RNG  $k-\varepsilon$  model (Yakhot and Orszag 1986) and the realizable  $k-\varepsilon$  model (Shih, *et al.* 1995), have been developed for the simulation of flows around bluff buildings, and the LES (Large Eddy Simulation) and the DNS (Direct Numerical Simulation) are believed to be tools of the future.

### Acknowledgements

Sponsored by National Natural Science Foundation of China(40333027) and LAPC Open Fund Project (LAPC-KF-2004-07)

### Appendix A - Introduction of the wind tunnel experiment of the effect of building clusters on flow structure<sup>[2]</sup>

This experiment was carried out in the NJU environment wind tunnel, which is a direct current, waftage neutral stratification wind tunnel, with a rectangle cross section. The width of experiment area is 2.0 m, the height is 1.4 m, and the length is 16 m. The frame of the wind tunnel is steel, the bottom is a wood footwall. Observation windows are located on the top wall and on one side wall. The experiment wind speed can be adjusted by 0.3–10 m/s continuously.

The spatial distributions of scale wind speed and turbulence energy are measured in the experiments. A DANTEC55 hot wire anemometer is fixed on a mobile shelf, which can move in three dimensions and is controlled by a PC. The building models (1:250 in scale) are placed on a circular plane, as shown in Fig. 20. The model height is 32 cm, corresponding to height of the real buildings, at 40 m. The wind speed and the turbulence intensities at the cross points are measured at the heights of 2 m, 20 m, and 44 m. The plane can be wheeled to change the direction of the inlet flows. The scale wind speeds are measure at a sample rate of

<sup>[2]</sup>More detailed information can be found in *Technology Report of the Research on Relations between Urban Design and Meteorological Conditions and Atmospheric Pollutant Dispersion in Beijing*, 2002

20 Hz, the sample time is 2 minutes, and the turbulence statistics may also be obtained.

## References

- Ashie, Y., Ca, W.T. and Asaeda, T. (1999), "Building canopy model for the analysis of urban climate", *J. Wind Eng. Ind. Aerody.*, **81**, 237-248.
- Baik, J.J. and Kim, J.J. (1999), "A numerical study of flow and pollutant dispersion characteristics in urban street canyons", *J. Applied Meteorology*, **38**, 1576-1589.
- Hosker, R.P. Jr (1985), "Flow around isolated structures and building clusters: a review", *ASHRAE Transactions*, **91**, 1671-1692.
- Hunter, L.J., Johnson, G.T. and Watson, I.D. (1992), "An investigation of three-dimensional characteristics of flow regimes within the urban canyon", *Atmospheric Environment*, **20**, 425-432.
- Hussain, M. and Lee, B.E. (1980), "A wind tunnel study of the mean pressure force acting on large groups of low-rise buildings", *J. Wind Eng. Ind. Aerody.*, **6**, 207-225.
- Hussein, H.J. and Martinuzzi, R.J. (1996), "Energy balance for turbulent flow around a surface mounted cube placed in a channel", *Physics Fluids*, **8**, 764-780.
- Kim, J.J. and Baik, J.J. (1999), "A numerical study of thermal effects on flow and pollutant dispersion in urban street canyons", *J. Applied Meteorology*, **38**, 1249-1261.
- Launder, B.E. and Spalding, D.B. (1974), "The numerical computation of turbulent flows", *Computer Methods in Applied Mechanics and Engineering*, **3**, 269-289.
- Murakami, S., Mochida, A. and Hayashi, Y. (1990), "Examining the  $k-\epsilon$  model by means of a wind tunnel test and large eddy simulation of the turbulence structure around a cube", *J. Wind Eng. Ind. Aerody.*, **35**, 87-100.
- Oke, T.R. (1988), "Street design and urban canopy layer climate", *Energy and Building*, **11**, 103-113.
- Patankar, S.V. (1980), *Numerical Heat Transfer and Fluid Flow*, New York, Hemisphere.
- Paterson, D.A. and Apelt, C.J. (1986), "Computation of wind flows over three-dimensional buildings", *J. Wind Eng. Ind. Aerody.*, **24**, 192-213.
- Paterson, D.A. and Apelt, C.J. (1989), "Simulation of wind flows around three-dimensional buildings", *Buildings Environment*, **24**, 39-50.
- Rotach, M.W. (1995), "Profiles of turbulence statistics in and above an urban street canyon", *Atmospheric Environment*, **29**, 1473-1486.
- Shih, T.H., Liou, W.W., Shabbir, A. and Zhu, J. (1995), "A new  $k-\epsilon$  eddy viscosity model for high Reynolds number turbulent flows-model development and validation", *Computers & Fluids*, **24**, 227-238.
- Sini, J.F., Anquetin, S. and Mestayer, P.G. (1996), "Pollutant dispersion and thermal effects in urban street canyons", *Atmospheric Environment*, **30**, 2659-2677.
- Yaknot, V. and Orszag, S.A. (1986), "Renormalization group methods in turbulence", *J. Science Computing*, **1**(1), 1-51.